nature COMMUNICATIONS

ARTICLE

Received 9 Apr 2014 | Accepted 24 Oct 2014 | Published 13 Jan 2015

DOI: 10.1038/ncomms6655

Reciprocal inhibition between sensory ASH and ASI neurons modulates nociception and avoidance in *Caenorhabditis elegans*

Min Guo[1,*], Tai-Hong Wu[1,*], Yan-Xue Song[1], Ming-Hai Ge[1], Chun-Ming Su[1], Wei-Pin Niu[1], Lan-Lan Li[1], Zi-Jing Xu[1], Chang-Li Ge[1], Maha T.H. Al-Mhanawi[1], Shi-Ping Wu[2] & Zheng-Xing Wu[1]

Sensory modulation is essential for animal sensations, behaviours and survival. Peripheral modulations of nociceptive sensations and aversive behaviours are poorly understood. Here we identify a biased cross-inhibitory neural circuit between ASH and ASI sensory neurons. This inhibition is essential to drive normal adaptive avoidance of a $CuSO_4$ (Cu^{2+}) challenge in *Caenorhabditis elegans*. In the circuit, ASHs respond to Cu^{2+} robustly and suppress ASIs via electro-synaptically exciting octopaminergic RIC interneurons, which release octopamine (OA), and neuroendocrinally inhibit ASI by acting on the SER-3 receptor. In addition, ASIs sense Cu^{2+} and permit a rapid onset of Cu^{2+}-evoked responses in Cu^{2+}-sensitive ADF neurons via neuropeptides possibly, to inhibit ASHs. ADFs function as interneurons to mediate ASI inhibition of ASHs by releasing serotonin (5-HT) that binds with the SER-5 receptor on ASHs. This elaborate modulation among sensory neurons via reciprocal inhibition fine-tunes the nociception and avoidance behaviour.

[1] Key Laboratory of Molecular Biophysics of Ministry of Education, Institute of Biophysics and Biochemistry, and Department of Biophysics and Molecular Physiology, College of Life Science and Technology, Huazhong University of Science and Technology, 1037 Luoyu Road, Wuhan 430074, China. [2] School of Chemical Engineering and Pharmacy, Wuhan Institute of Technology, Wuhan 430073, China. * These authors contributed equally to this work. Correspondence and requests for materials should be addressed to Z.-X.W. (email: ibbwuzx@mail.hust.edu.cn).

Sensory neurons transform various stimuli from the external and internal environment into sensory information that is primarily integrated in the central nervous system to form sensation and perception, drive adaptive behaviours and maintain physiological homeostasis. The sensory modulations at the level of sensory neurons or the initial chain of sensory pathways are important for animals to achieve direct, fast and more fine-tuned regulation of sensations and behaviours[1–3]. Owing to feasible genetic manipulation, a simple and stereotyped nervous system, the nematode *Caenorhabditis elegans* is a good animal model for the study of peripheral modulation of sensations. In *C. elegans*, nociceptive sensations and avoidance have been intensively studied. However, the reported studies were focused on the functional mapping of the connections among sensory neurons and interneurons, using cell ablation, optogenetic manipulation and *in vivo* calcium imaging[4–7]. Therefore, the peripheral modulation of nociceptive sensations and avoidance behaviours is poorly understood.

The polymodal ASH sensory neurons in *C. elegans* sense a variety of aversive stimuli and mediate avoidance of high osmotic, mechanical and chemical stimuli[8–11]. Notably, the neurotransmitters, such as neuropeptides, serotonin (5-HT), tyramine (TA) and octopamine (OA), have been increasingly shown to be transmitters or modulators of ASH-mediated aversive behaviours[12–15]. ASI sensory neurons are reported to mediate dauer formation[16], enable worms to learn to avoid the smell of pathogenic bacteria after ingestion via INS-6 signalling[17], suppress male-specific sexual attraction behaviour[18], respond to temperature stimuli to negatively modulate thermotaxis behaviour[19], mediate diet-restriction-induced longevity[20], modulate satiety quiescence[21], regulate acute CO_2 avoidance[22], repress exploratory behaviours that comprise spontaneous reversals and omega turns[5], and inhibit ASH-mediated aversive responses to 100% 1-octanol[23]. These studies support the hypothesis that ASIs are important polymodal sensory neurons mediating or modulating worm behaviours and development.

Here, using a reverse genetic screen as well as genetic manipulation, quantitative behaviour assays, *in vivo* Ca^{2+} imaging and neuronal manipulation, we determine that reciprocal inhibition between ASHs and ASIs exists following a challenge of nociceptive Cu^{2+} stimulation and identify the underlying molecular mechanism and neural circuit. The elaborate modulation of Cu^{2+} sensation through the reciprocal inhibitory neuron circuit fine-tunes the worm nociception and avoidance behaviour.

Results

Blocking ASH and ASI alters kinematics of $CuSO_4$ reversal. A wild-type *C. elegans* worm exhibits a rapid backward movement when its nose encounters water-soluble repellents in a dry drop test[24]. To quantify the kinematics of worm undulatory locomotion during a $CuSO_4$-evoked reversal, we calculated the normalized curvature (NC) of the worm body[25,26]. In brief, the worm body was divided into ten equal segments from head to tail (head = 0 and tail = 1). The NC of each point along the body centre line was defined as the total length of the body centre line (L) divided by the radius of curvature (R) of the point (Fig. 1a). Typically, as the absolute value of the NC increases, the bending magnitude increases. We used a quadrant assay with some modifications[27], to test the sensitivity of mass worms to $CuSO_4$ (Fig. 1b). Whereas a wild-type worm exhibited no obvious response to M13 buffer in the dry drop test (Supplementary Movie 1), it generated a continuous and rhythmic sinusoidal backward locomotion when challenged with 10 mM $CuSO_4$-M13 buffer solution (Fig. 1c1 and Supplementary Movie 2). The bending magnitude of the reversal in the tail was stronger than that in the head (Fig. 1d1), which was different from previously reported forward locomotion[26].

To identify the functions of ASI and ASH neurons in the Cu^{2+}-evoked avoidance behaviour, we used the light chain of tetanus toxin (TeTx) to block ASI and ASH neurotransmission (silence or block neurons for short)[28]. TeTx is a specific protease of synaptobrevin and has been used successfully to inhibit chemical synaptic transmission in *C. elegans*[29]. We examined the impact of silencing ASIs on the kinematics of a Cu^{2+}-evoked reversal. We observed a marked increase in the duration and body bends of the backward movements (Fig. 1c2,e,f and Supplementary Movie 3), but no change in the bending magnitude (Fig. 1d2) compared with those observed in wild-type animals. We next examined the changes in the sensitivity of mass worms to Cu^{2+} stimulations using the quadrant assay. Our result showed that worms displayed hypersensitivity after permanently blocking ASI neurotransmission with TeTx (Fig. 1g). We then explored the effects of blocking ASHs on the reversal kinematics. No ASH-specific promoter has been identified; therefore, we used a flippase (FLP)-flippase recognition target (FRT) site-specific recombination system to drive specific expression of TeTx in ASH neurons[29,30]. When worms expressed both *sra-6p::flp-sl2-flp::3′UTR* and *gpa-11p::frt-stop-frt::TeTx::sl2-GFP* constructs, FLP recombinase driven by the *sra-6* promoter excised the FRT-flanked transcriptional terminator. This allowed specific expression of TeTx and a green fluorescent protein (GFP) fluorescence marker in ASH neurons that possess a combinatorial intersection between *sra-6* and *gpa-11* promoters[30] (Fig. 1h). Specifically silencing ASH neurons significantly decreased the bending magnitude of the worm anterior body region (Fig. 1c3,d3 and Supplementary Movie 4), had no impact on the duration and the body bend of the reversal (Fig. 1e,f), and also significantly decreased the sensitivity to Cu^{2+} of the mass worms measured by the quadrant assay (Fig. 1g). These results demonstrated that ASHs are nociceptive Cu^{2+} sensory neurons and play an important role in anterior body bending as part of the Cu^{2+} avoidance behaviour. Interestingly, blocking both ASH and ASI neurons induced a serious uncoordinated reversal and even irreversible backward locomotion. Only bends of weak magnitude remained in the anterior parts of the body (Fig. 1c4,d4,e,f and Supplementary Movie 5).

ASIs inhibit ASHs to regulate worm aversive behaviour. As blocking ASI affects worm aversive behaviour and sensitivity to Cu^{2+}, we next addressed the underlying mechanism. We first monitored Ca^{2+} transients in ASHs using the genetically encoded Ca^{2+} sensor R-GECO1 (Fig. 2a), which has properties of high Ca^{2+} affinity, a large dynamic range and slow photobleaching[31]. A transparent polydimethylsiloxane microfluidic device was used to trap and expose worms to the Cu^{2+} stimulus[32,33]. ASHs showed an obvious on- and off-response that precisely corresponded to the presentation and removal of the noxious stimulus, respectively, following a 30-s stimulation with 10 mM $CuSO_4$ (Fig. 2b, Supplementary Fig. 1 and Supplementary Movie 6). However, ASIs showed only an off-response of Ca^{2+} transient but no apparent on-response (Fig. 2c and Supplementary Movie 7). We employed TeTx to permanently block ASI neurotransmission, and ArchT, a light-driven outward proton pump with high light sensitivity[34], to optogenetically inhibit ASI neurons. Genetically silencing and optogenetically inhibiting ASIs (Fig. 2c) significantly prolonged the on-response of Cu^{2+}-elicited Ca^{2+} signals in ASH neurons (Fig. 2b and Supplementary Movie 8). As expected, the optogenetic inhibition, but not the genetic blocking, markedly decreased ASI off-response Ca^{2+} signals, suggesting that TeTx

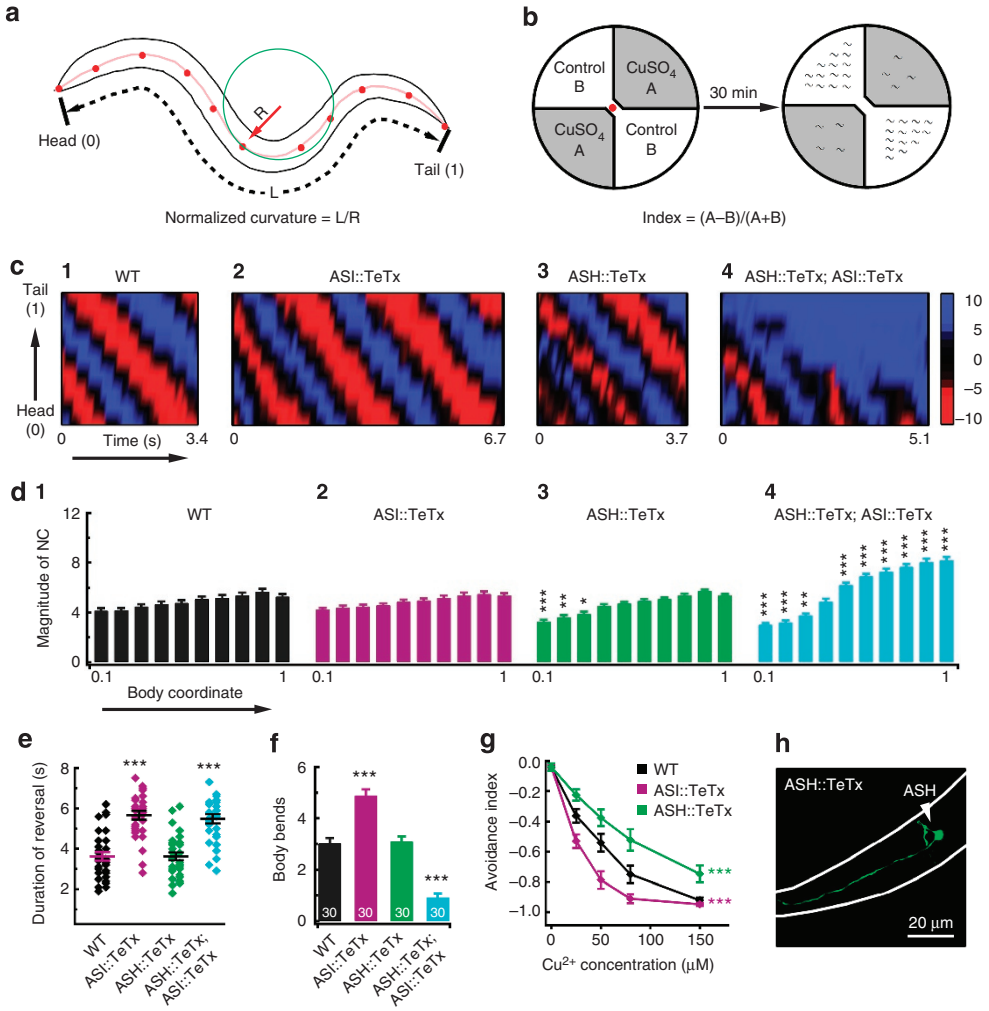

Figure 1 | Sensory neurons ASHs and ASIs direct the Cu^{2+}-evoked avoidance behaviour. (**a**) Schematic representation of quantification of NC along the body centre line. The length of body centre line *L* is divided into 10 equal segments from head (0) to tail (1) using 11 points. The radius of curvature *R* at the middle point of a segment is defined as the curvature of this segment. The non-dimensional NC was calculated by dividing the *L* by *R*. (**b**) Schematic representation of a modified quadrant assay. The red dot represents the starting point of the worms. (**c1**–**c4**) Kymograms of the time-dependent NC along the body centre line of Cu^{2+}-evoked reversals in the worms after blocking different neurons by neuron-specific expression of TeTx. The data are expressed as means, $n=30$ assays. The vertical axis represents the midline of body from head (0) to tail (1) in non-dimensional units, and the horizontal axis represents the duration of the reversal. (**d1**–**d4**) The magnitude of body bend described in **c1**–**c4**. NC indicates normalized curvature and similarly hereinafter; $n=30$ assays. The durations (**e**) and body bends (**f**) of the Cu^{2+}-elicited reversal assayed by the dry drop test in the worms after blocking neurotransmission in different neurons. The number on each bar indicates the number of independent tests for each genotype. (**g**) The worm avoidance indexes in response to various concentrations of Cu^{2+} tested by the quadrant assay, that is, Cu^{2+} sensitivity, $n \geq 8$ assays. (**h**) The specific expression of TeTx light chain in ASHs using a FLP-FRT site-specific recombination system. Scale bar, 20 μm. The data except those in **c** are expressed as means ± s.e.m. Two-way analysis of variance (ANOVA) test in **d1**–**d4** and **g**, and one-way ANOVA test in **e**,**f**. Corrected with Bonferroni *t*-test for multiple comparisons (*$P \leq 0.05$, **$P \leq 0.01$ and ***$P \leq 0.001$ compared with the wild-type N2 control).

blocked neurotransmission but did not change ASI excitation (Fig. 2c).

We next examined the effect of activating ASIs on ASH Cu^{2+}-evoked Ca^{2+} signals. Worms display phototaxis[35]. Thus, to avoid the possible interference from light used in optogenetics, we employed chemical genetics using transient receptor potential vanilloid 1 (TRPV1), a mammalian cation channel activated by an exogenous ligand capsaicin, to chemogenetically activate ASI neurons[36]. Our results showed that the expression of rat TRPV1 endowed ASIs with the ability to respond to the application of 100 μM capsaicin (Fig. 2d). The chemogenetic activation of ASIs significantly decreased the ASH Ca^{2+} transients in response to the Cu^{2+} challenge (Fig. 2e). Moreover, artificially activating ASIs induced the identical changes in Cu^{2+} sensitivity (Fig. 2f,g), no changes in the duration of reversal and body bend (Fig. 2h,i), and similar but more severe changes in the bending magnitudes in the anterior parts of the body (Fig. 2j) compared with blocking ASH neurons. Taken together, these results demonstrate that ASIs inhibit the ASH response to Cu^{2+} and regulate the worm Cu^{2+} avoidance behaviour.

5-HT mediates ASI inhibition on ASHs via the SER-5 receptor. ASIs are presynaptic to ASHs (www.wormweb.org). For identifying ASI neural signalling, we used reverse genetics to screen neuropeptide and neurotransmitter receptors, using a standard that Cu^{2+}-evoked Ca^{2+} signals of ASHs were similar to those in ASI-blocked worms (Supplementary Fig. 2). We found that the *ser-5* loss-of-function (lof) mutations (*ser-5*(*ok3087*) and *ser-5*(*tm2647*)) had similar impacts to permanently silencing ASIs

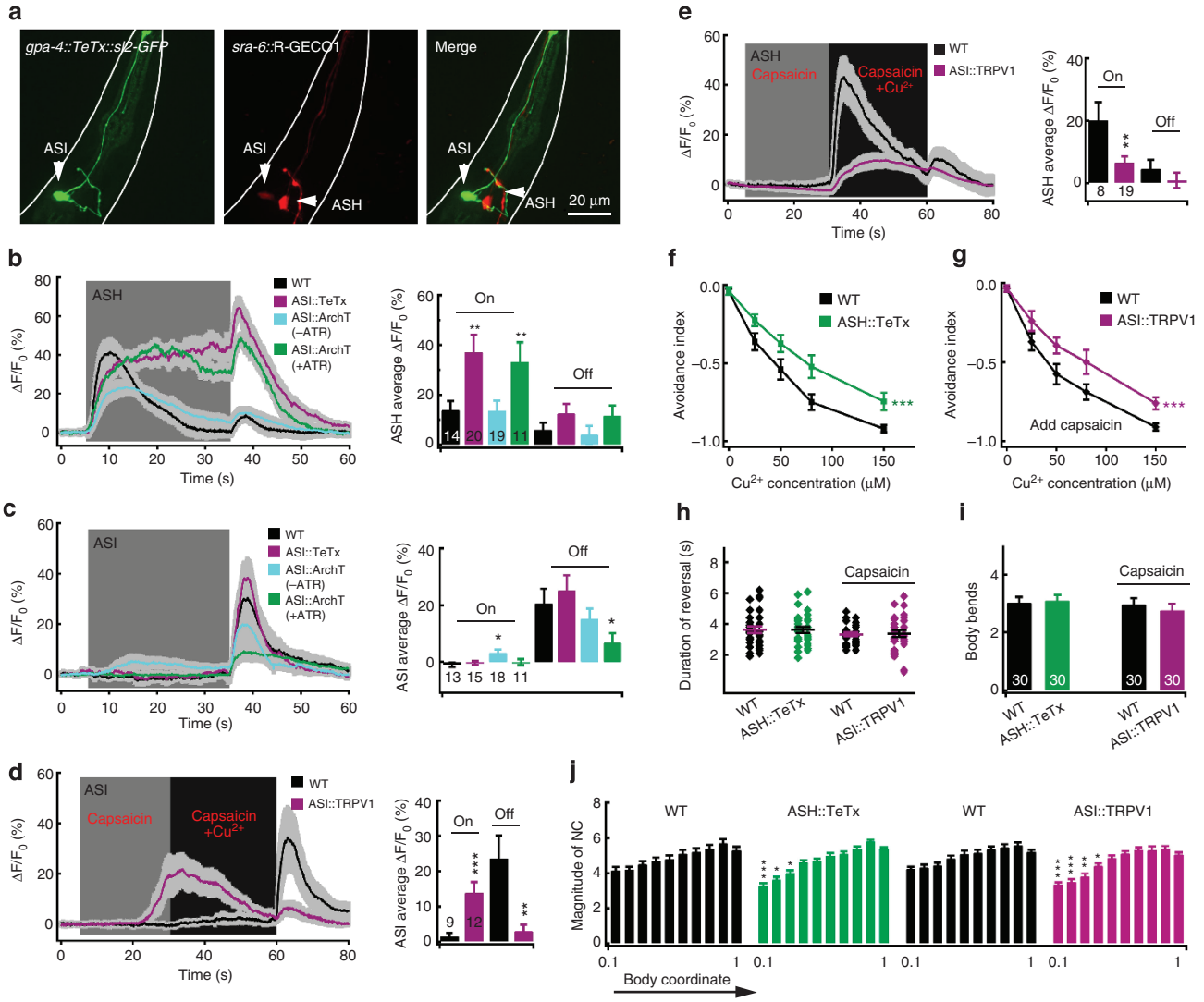

Figure 2 | ASIs inhibit ASH Cu^{2+}-elicited Ca^{2+} response and worm avoidance. (**a**) Expression of TeTx in ASIs and R-GECO1 in ASHs. Scale bar, 20 μm. ASH (**b**) and ASI (**c**) Ca^{2+} responses to a 10-mM Cu^{2+} stimulation after blocking or during optogenetic inhibition of neurotransmission in ASIs. 'On' and 'Off' indicate Ca^{2+} signals to the presentation and removal of the Cu^{2+} stimulation, respectively. For calculating the ratio of $\Delta F/F_0$, the ΔF and F_0 for the on-response are defined as the fluorescence changes during the application of $CuSO_4$ and the average fluorescence intensity of 5 s before the Cu^{2+} stimulation, and the ΔF and F_0 for off-response are defined as the initial fluorescence changes 5 s after the removal of $CuSO_4$ and the average fluorescence intensity of the last 5 s of the on-response, respectively. Grey shading denotes the period of Cu^{2+} application. For ArchT optogenetic inhibition, continuous green light irradiation was applied during the entire recording, ATR, all-trans-retinal; similarly herein after. The ASI (**d**) and ASH (**e**) Ca^{2+} signals in response to the 10 mM $CuSO_4$ stimulation following chemogenetic activation of ASIs. Neurons that specifically expressed TRPV1 were activated by exogenous capsaicin (100 μM). The F_0 of the on-response was defined as the average fluorescence intensity from 0 to 5 s. Light grey and dark grey shading denote the span of applications of capsaicin and capsaicin plus Cu^{2+}, respectively; similarly herein after. Comparison of Cu^{2+} sensitivity tested by the quadrant assay (**f**,**g**, $n \geq 8$ assays) and kinematics of the Cu^{2+}-evoked reversal in the dry drop test (**h**–**j**, $n = 30$ assays) after genetically blocking ASHs with TeTx or chemogenetically exciting ASIs with TRPV1 plus 10 μM capsaicin. All data are expressed as means ± s.e.m. The number on each bar indicates the number of independent tests for each genotype. One-way analysis of variance (ANOVA) test in **b**–**e** and **h**,**i**, and two-way ANOVA test in **f**,**g**,**j**. Corrected with Bonferroni *t*-test. Statistical significance was indicated as: $^*P \leq 0.05$, $^{**}P \leq 0.01$ and $^{***}P \leq 0.001$.

on ASH Cu^{2+}-elicited Ca^{2+} signals (Fig. 3a and Supplementary Fig. 2), the kinematics of Cu^{2+}-evoked reversal (Fig. 3b,c) and Cu^{2+} sensitivity (Fig. 3d), and these mutations also had no effect on the bending magnitudes (Supplementary Fig. 3a). All defects in the mutants were rescued by the ectoexpression of *ser-5* genomic DNA driven by its own or ASH-specific promoter in *ser-5*(*ok3087*) (Fig. 3a–d and Supplementary Fig. 3a). Genetically blocking ASIs and the *ser-5* lof mutation had no impact on ASI Cu^{2+}-elicited Ca^{2+} signals as expected (Supplementary Fig. 3b). These data suggested that SER-5 directly mediated ASI inhibition of the ASH Cu^{2+} response and thus worm aversive behaviour. *ser-5* encodes a 5-HT receptor, which is widely expressed in head neurons including ASHs[37] (Fig. 3e). We then tested whether blocking the biosynthesis of 5-HT causes phenotypes similar to the lof mutation of *ser-5*. The gene *tph-1* encodes tryptophan hydroxylase that catalyses the rate-limiting first step in 5-HT biosynthesis[38]. In the *C. elegans* hermaphrodite, *tph-1* expression is limited to only a few serotonergic neurons, such as NSMs, ADFs and HSNs, and rarely in AIMs and RIH (Supplementary Fig. 3c). Indeed, in *tph-1*(*mg280*) mutants, which fail to synthesize 5-HT, the ASH calcium transients and the avoidance behaviours were similar to those in the *ser-5*-null mutants (Fig. 3f,h–j and

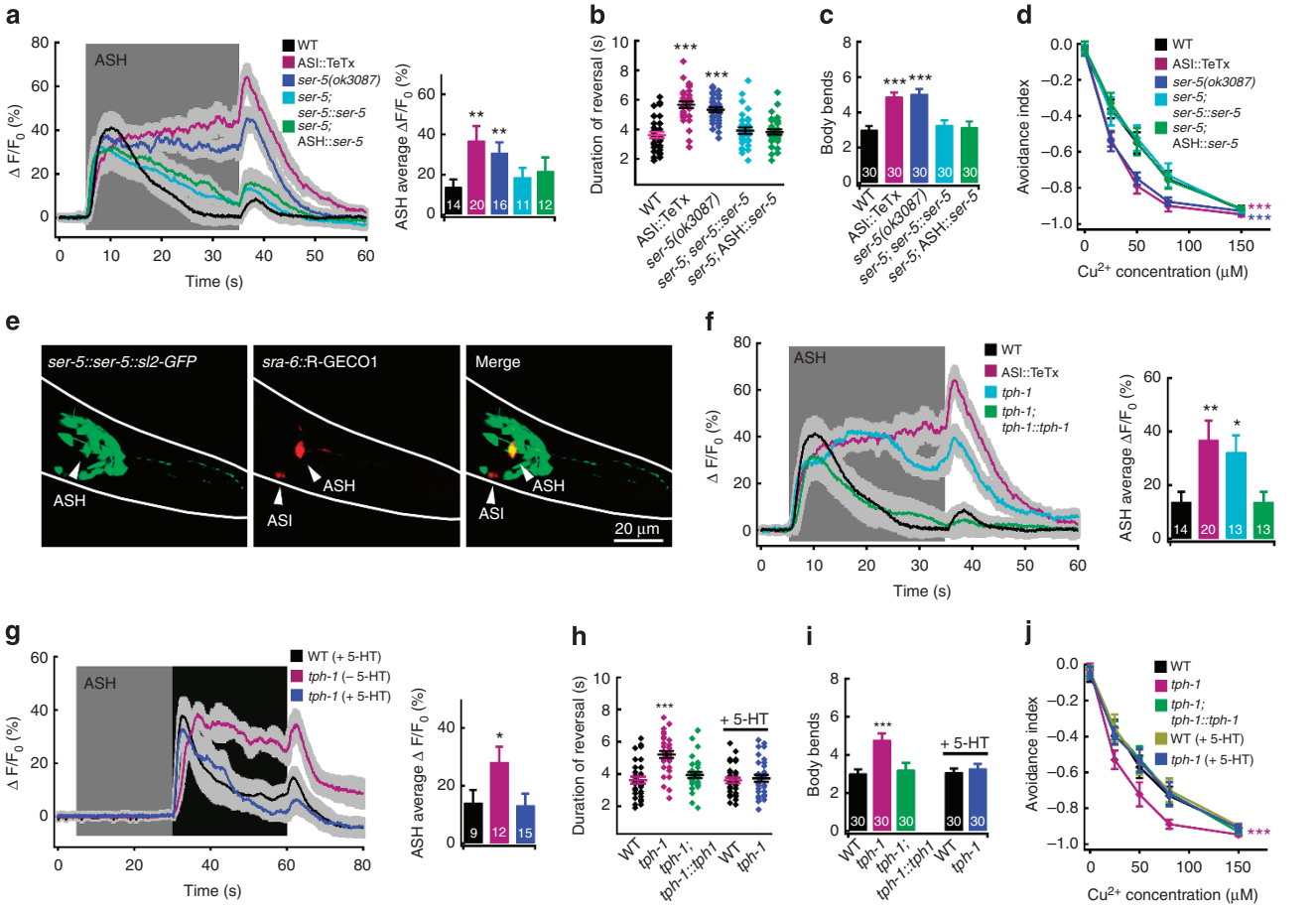

Figure 3 | 5-HT and the SER-5 receptor transduce ASI inhibition of ASHs. (**a**) ASH calcium responses to 10 mM $CuSO_4$ in wild-type, ASI neurotransmission blocked, *ser-5* mutant, and *ser-5p*::*ser-5* and ASH::*ser-5* genetically rescued worms. Summation of the kinematics of Cu^{2+} avoidance behaviours (**b**,**c**) and Cu^{2+} sensitivity (**d**, $n \geq 8$ assays) in the worms mentioned above. (**e**) The expression pattern of *ser-5p*::*ser-5*::*sl2-GFP* and *sra-6p*::*R-GECO1* in *ser-5*-null mutants. These genes were co-expressed in ASH neurons. Scale bar, 20 μm. (**f**) The *tph-1* lof mutation had a similar effect on the ASH Cu^{2+}-elicited Ca^{2+} signals as did genetically silencing ASI with TeTx, and the defect was rescued by *tph-1p*::*tph-1* ectoexpression. (**g**) The defect of the ASH Ca^{2+} transients in the *tph-1* mutants was rescued by application of 5 mM exogenous 5-HT. Summation of the kinematics of Cu^{2+} avoidance behaviours (**h**,**i**) and Cu^{2+} sensitivity (**j**, $n \geq 8$ assays) in the worms denoted. All data are expressed as means ± s.e.m. The number on each bar indicates the number of independent tests for each genotype. One-way analysis of variance (ANOVA) test in **a**–**c** and **f**–**i**, and two-way ANOVA test in **d** and **j**. Corrected with Bonferroni *t*-test. Values that differ significantly are indicated (*$P \leq 0.05$, **$P \leq 0.01$ and ***$P \leq 0.001$ compared with the wild-type N2 control).

Supplementary Fig. 3d). The defects were rescued by the expression of *tph-1* directed by its own promoter or the application of 5 mM exogenous 5-HT (Fig. 3f–j and Supplementary Fig. 3d). These results suggest that endogenous 5-HT mediates ASI inhibition of ASH neurons. Taken together, our results suggest that endogenous 5-HT directly acts on the SER-5 receptor to mediate the ASI inhibition of ASHs. However, as ASIs are not known to be serotonergic neurons, exactly which neurons release the 5-HT that regulates the ASH response and worm avoidance behaviour needs further investigation.

ADFs act as interneurons to mediate ASI inhibiting ASHs. Among serotoninergic neurons, NSMs, AIMs and RIH showed no Cu^{2+}-evoked Ca^{2+} signals in wild-type and ASI-blocked worms (Supplementary Fig. 4a–c). Only ADF neurons showed a Cu^{2+}-evoked Ca^{2+} response. Furthermore, the onset of the Ca^{2+} signals was delayed by silencing ASIs (Fig. 4a), suggesting that ADFs probably relayed ASI inhibition to ASHs. To validate the ADF intermediate function, we examined the impact of optogenetically inhibiting ASIs on Cu^{2+}-evoked Ca^{2+} signals of ADFs. As expected, the Ca^{2+} response in ADFs was significantly delayed by specific optogenetic inhibition of ASIs, but the intensity was not altered (Fig. 4a). We further employed *unc-13* lof mutation to validate the observation. As the gene *unc-13* is essential for synaptic vesicle exocytosis and neurotransmitter release[39,40], the lof mutants were used to analyse the sensational response in sensory neurons under neuronal isolation[41,42]. Our data showed the lof mutation of *unc-13*(*e1091*) had a similar impact on ADF Cu^{2+}-elicited Ca^{2+} transients to genetically blocking or optogenetically inhibiting ASIs (Fig. 4b), suggesting that sensory ADF neurons may probably be sensitive to Cu^{2+}. We then tested whether artificial activation of ASI promotes a more rapid onset of the Ca^{2+} response in ADFs. Unexpectedly, chemogenetic activation of ASIs with 100 μM capsaicin had no apparent impact on the Ca^{2+} signals in ADFs with (Supplementary Fig. 4d, 5–30 s) or without (Supplementary Fig. 4d, 30–60 s) the Cu^{2+} stimulation. Prolonged direct chemogenetic activation of ADFs (55 s) without $CuSO_4$ resulted in no apparent ADF Ca^{2+} transients in the ASI-blocked worms and very slowly appearing Ca^{2+} transients in the ASI-undisrupted worms (Supplementary Fig. 4e). In addition,

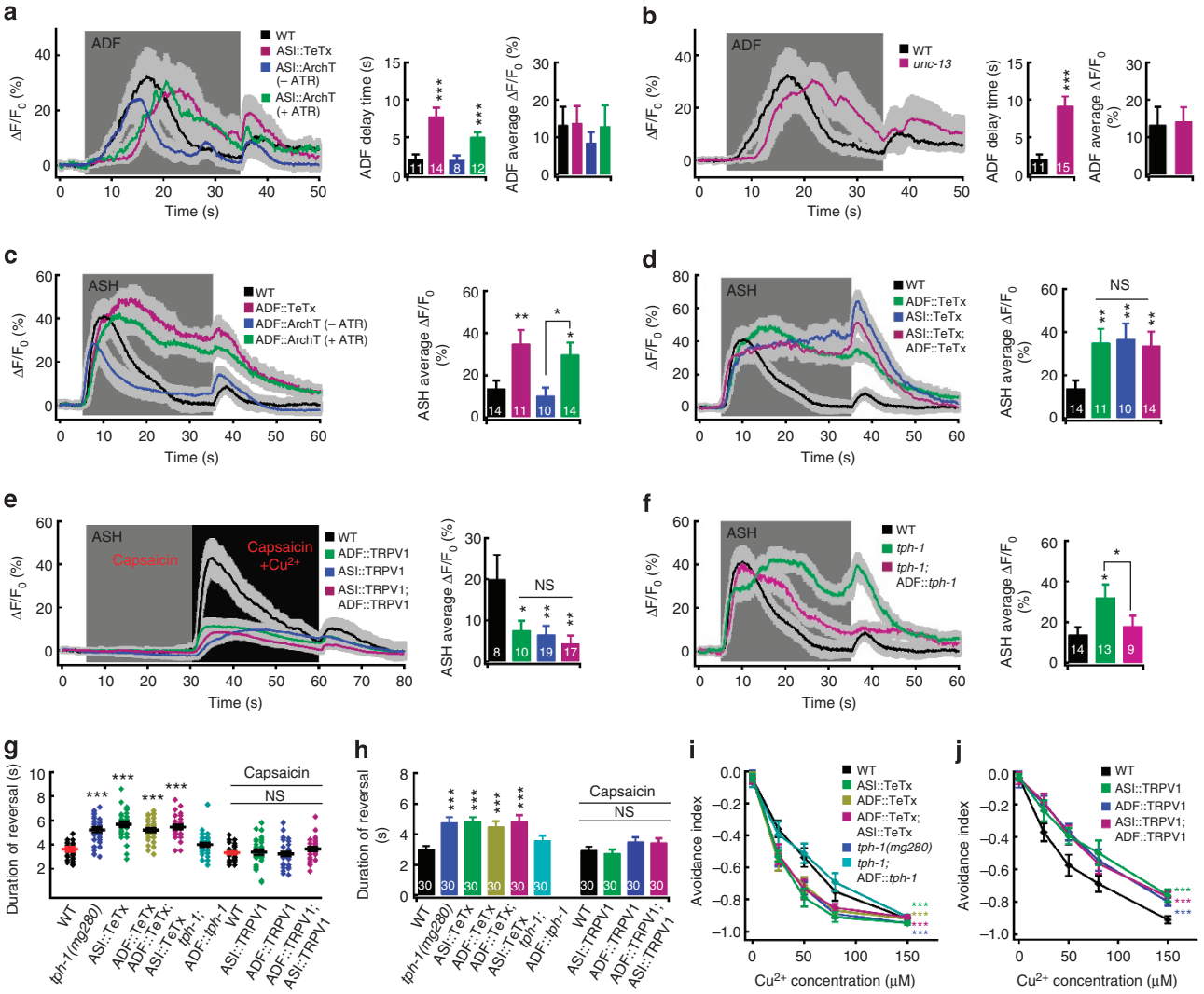

Figure 4 | ADF neurons mediate ASI inhibition of ASHs. ADF Ca^{2+} responses to the 10 mM $CuSO_4$ stimulation in the ASI-silenced and ASI-opto-inhibited worms (**a**), and *unc-13* mutants (**b**). The delay time was calculated as the time of stimulus application to the time when the single-exponential fitted curve of individual Ca^{2+} on-response trace cuts fitted straight line of basal Ca^{2+} signals before stimulation. (**c**) Genetically blocking and optogenetically inhibiting ADF neurons similarly prolonged the ASH Cu^{2+}-evoked Ca^{2+} signals. Silencing ASIs, ADFs and both types of neurons with TeTx had similar effects on the ASH Cu^{2+}-elicited Ca^{2+} transients (**d**) and chemogenetically activating ASIs, ADFs and both types of neurons also had the similar effects on the ASH Ca^{2+} signals (**e**). The neuron expressing rat TRPV1 cation channels was activated by the application of 100 μM capsaicin. (**f**) ASH Ca^{2+} response to the 10 mM Cu^{2+} stimulation in *tph-1* mutants and in ADF::*tph-1* genetically rescued worms. The durations (**g**) and body bends (**h**) of the Cu^{2+}-evoked reversal in wild-type N2 and the neuronal manipulated worms assayed by the dry drop test. (**i**) Similar effects on animal Cu^{2+} sensitivity were observed among *tph-1* lof mutation that were rescued by its ADF expression, genetically silencing and optogenetically inhibiting ASIs, ADFs and both types of neurons ($n \geq 8$ assays). (**j**) Chemogenetically activating ASIs, ADFs and both types of neurons had similar effects on animal Cu^{2+} sensitivity ($n \geq 8$ assays). All data are expressed as means ± s.e.m. The number on each bar indicates the number of independent tests for each genotype. One-way analysis of variance (ANOVA) test in **a**–**h** and two-way ANOVA test in **i** and **j**. Corrected with Bonferroni *t*-test. Values that differ significantly are indicated (*$P \leq 0.05$, **$P \leq 0.01$ and ***$P \leq 0.001$; n.s., not significant compared with the wild-type N2 control or as indicated).

chemogenetically activating ADFs evoked no apparent Ca^{2+} signal without the Cu^{2+} stimulation (Supplementary Fig. 4f, 5–30 s), and did not change the ASI promotion of ADF Cu^{2+}-evoked Ca^{2+} signals, if compared the delay time and amplitude of their Ca^{2+} signals (Supplementary Fig. 4f, 30–60 s) with those in the ADF-undisturbed worms (Fig. 4a). These results suggest that ASIs do not directly activate ADFs, but instead permit a more rapid onset of Cu^{2+}-elicited Ca^{2+} responses in ADFs and also support that ADFs are Cu^{2+} sensitive.

We expected that manipulating ADFs would have the same effects on the ASH calcium transients and worm Cu^{2+}-elicited avoidance behaviours as did manipulating ASIs. Indeed, as anticipated, blocking or inhibiting ADF neurotransmission by TeTx or ArchT, significantly enhanced ASH Ca^{2+} signals (Fig. 4c), and blocking ADFs, ASIs and both pairs of neurons had no significant difference in their effects on the ASH Ca^{2+} signals (Fig. 4d). Chemogenetically activating ASIs, ADFs and both types of neurons with only the application of capsaicin had no effect on Cu^{2+}-unstimulated ASHs (Fig. 4e, 5–30 s), but inhibited ASH Cu^{2+}-evoked Ca^{2+} responses similarly (Fig. 4e, 30–60 s). These results confirm that ADFs mediate the ASI inhibition of ASHs.

The *tph-1* lof mutation was expected to have a similar effect on ASH Cu^{2+}-elicited Ca^{2+} signals as did blocking ASI and should be rescued by the expression of the gene in ASHs. As expected,

tph-1(*mg280*) mutants showed an augmented Ca^{2+} transient and the defect was rescued by the specific expression of *tph-1* in ADF neurons (Fig. 4f). Furthermore, inhibition of ADFs, ASIs, both types of neurons and the *tph-1* lof mutation had very similar effects on aversive behaviours tested by the dry drop and the worm Cu^{2+} sensitivities assayed by the quadrant assay (Fig. 4g–i and Supplementary Fig. 4g). In addition, chemogenetically activating ADFs, ASIs and both types of neurons also had similar effects on Cu^{2+} avoidance and Cu^{2+} sensitivity (Fig. 4g,h,j and Supplementary Fig. 4h).

ADFs are postsynaptic neurons of ASHs (www.wormweb.org) and they may receive neural signals directly from ASHs. We then positively (Supplementary Fig. 5a) and negatively manipulated ASH neurons and examined the changes of Ca^{2+} transients in ADFs to test the hypothesis. Chemogenetic activation of ASHs with TRPV1 plus capsaicin did not change ADF activity (Supplementary Fig. 5b). Permanently blocking ASHs with TeTx, optogenetically inhibiting ASH with ArchT and chemogenetically inhibiting ASHs with the *Drosophila* HisCl1 channel[43] plus 30 mM histamine also had no effect on Cu^{2+}-elicited Ca^{2+} transients in ADFs (Supplementary Fig. 5c–h). Moreover, blocking both ASIs and ASHs had a similar effect on ADF Cu^{2+}-evoked Ca^{2+} signals to blocking ASI alone (Supplementary Fig. 5i,j). These results exclude the possibility that ADFs receive neural signals from ASHs, which then feed back to inhibit ASHs. Taken together, ASIs advance sensory serotonergic ADF excitation to release the neurotransmitter 5-HT that inhibits ASH neurons during the Cu^{2+} stimulation.

ASIs are neuropeptidergic neurons (www.wormatlas.org). To test whether neuropeptides mediate the neurotransmission between ASIs and ADFs, we used mutants that have defects in neuropeptide release and biogenesis. *unc-31* is necessary for neuropeptide release from dense cored vesicles[44,45]. In *unc-31*(*e928*) mutants, ADFs showed a delayed onset of Cu^{2+}-evoked Ca^{2+} transients (Supplementary Fig. 6a). The *egl-3* gene encodes a homologue of a mammalian proprotein convertase that participates in peptide secretion[46] and the *egl-21* gene encodes a putative carboxypeptidase that is required for normal synthesis of FMRFamide-like peptides and neuropeptide-like peptides[47]. Our data showed that the lof mutations of *egl-3* (*egl-3*(*tm1377*)) and *egl-21* (*egl-21*(*n476*)) postponed the ADF Ca^{2+} signals (Supplementary Fig. 6b). We also observed significant defects in the ADF Ca^{2+} signals in *nlp-5*, *ins-1* and *ins-3* mutants (Supplementary Fig. 6c). These data suggest that neuropeptides most probably mediate the neurotransmission between ASIs and ADFs. Altogether, our results strongly support that sensory ASI neurons sense Cu^{2+} and permit ADFs to accelerate the onset of ADF activity during the Cu^{2+} stimulation for 30 s. Sensory ADF neurons sense Cu^{2+} stimulation and release 5-HT to inhibit ASHs.

SER-3 receptor intermediates ASH inhibiting ASIs. Direct activations of ASIs by photogenetic stimulation with ChR2 (ref. 6) and a high K^+ solution[42] evoke continuously increasing Ca^{2+} signals other than only an off- but no obvious on-response of Cu^{2+}-evoked Ca^{2+} transients under physiological condition, suggesting that ASI neurons receive inhibitory signals from other neurons. ASIs inhibit ASHs during Cu^{2+} stimulation, but whether ASHs inhibit ASIs to form a reciprocal inhibition circuit remained unclear. To answer this question, we first examined the effects of blocking (Fig. 5a) and inhibiting ASHs on Cu^{2+}-elicited Ca^{2+} signals in ASIs. Our results showed that permanently blocking or temporarily opto-inhibiting ASHs resulted in an obvious on-response of Cu^{2+}-evoked Ca^{2+} signals in ASIs (Fig. 5b and Supplementary Movie 9). As expected, ASH Cu^{2+}-elicited Ca^{2+} signals were reduced by opto-inhibition with ArchT but were not disturbed by the permanent block with TeTx (Supplementary Fig. 7a). These results suggest that the ASI on-response is inhibited by ASHs.

ASHs are postsynaptic but not presynaptic cells of ASIs[48]. Therefore, it is likely to be that ASH neurons modulate ASIs via a mediator. We then explored the molecular mechanism underlying the ASH inhibiting ASIs, employing the same strategy used in identifying the SER-5 receptor. We found that ASI Ca^{2+} on-responses in *ser-1*(*ok345*), *ser-3*(*ad1774*), *ser-3*(*ok1995*) and *tyra-2*(*tm1815*) mutants were similar to those in the ASH-silenced worms (Supplementary Fig. 8), but only *ser-3* mutants were rescued by extrachromosomal expression of the gene driven by its own or an ASI-specific promoter (Fig. 5c). These results suggest *ser-3* probably mediated the ASH inhibition of ASIs. The gene *ser-3* encodes an OA receptor that is widely expressed in a number of head and tail neurons including ASIs[14] (Fig. 5d). The Cu^{2+} evoked avoidance behaviour and Cu^{2+} sensitivity in *ser-3* mutants were also similar to those in the ASH-blocked worms, and were rescued by its own or an ASI-specific promoter (Fig. 5e and Supplementary Fig. 7b–d). These data suggest that SER-3 directly functions in ASI neurons to mediate the ASH inhibition of ASIs.

Octopaminergic RIC neurons mediate ASH inhibiting ASIs. Because *ser-3* encodes an OA receptor, we next tested whether OA is the ligand that mediates the ASH inhibition of ASIs. We checked the *tbh-1*(*n3247*) mutants that are unable to biosynthesize OA[49,50]. In the mutants, the Cu^{2+}-elicited on-response of Ca^{2+} signals in ASIs was significantly augmented, although the amplitudes were smaller than those observed in the ASH-blocked worms (Fig. 6a,b). Specific expression of *tbh-1* driven by its own promoter in RIC neurons fully rescued the defects in the ASI Ca^{2+} signals (Fig. 6a). As RICs have no synaptic connection with ASIs[48], RICs probably function as neuroendocrine cells to mediate the ASH inhibition of ASIs.

TA is an intermediate in the synthesis of OA[49,50]. To test whether TA has the same function as OA, we used *tdc-1*(*n3419*) mutants that fail to biosynthesize both TA and OA. We examined the Cu^{2+}-evoked avoidance behaviour in the mutants. Our data showed that the *tdc-1*(*n3419*) worms exhibited the similar defects in the Cu^{2+}-evoked aversive behaviour and Cu^{2+} sensitivity to the *tbh-1* mutants (Supplementary Fig. 9a–d), suggesting that TA did not probably mediate the ASH modulation of ASIs.

ASH neurons connect with RICs by gap junctions[48]. To further confirm the intermediate function of RICs in ASH inhibiting ASIs, we employed TeTx (Fig. 6b) to permanently block ASH neurotransmission, or ArchT to optogenetically inhibit ASHs. Our results showed that the Ca^{2+} transients of RICs were significantly reduced in ASH-inhibited worms and even reversed in the ASH-blocked animals (Fig. 6c). The gene *unc-9* encodes an innexin, an integral transmembrane channel protein that is a structural component of invertebrate gap junctions, which is expressed in RICs[51] (Supplementary Fig. 9e). The *unc-9* mutation (*unc-9*(*e101*)) had similar effect on RIC Cu^{2+}-elicited Ca^{2+} signals as did the negative manipulation of ASHs with TeTx and ArchT (Fig. 6c). In addition, the lof mutation of another innexin encoding gene *inx-4* (in *inx-4(e1128)*) had a similar phenotype to the *unc-9* mutation (Supplementary Fig. 9f). These data suggest that permanent expression of TeTx most probably disrupts neurotransmission through the gap junctions.

Direct manipulation of RICs would have the same effect on ASI Cu^{2+}-evoked Ca^{2+} signals as manipulating ASHs. Indeed, negative manipulation of RICs with TeTx and ArchT affected the ASI Ca^{2+} transients (Fig. 6d and Supplementary Fig. 9g) similar to blocking and inhibiting ASHs (Fig. 5b). In addition, the RIC

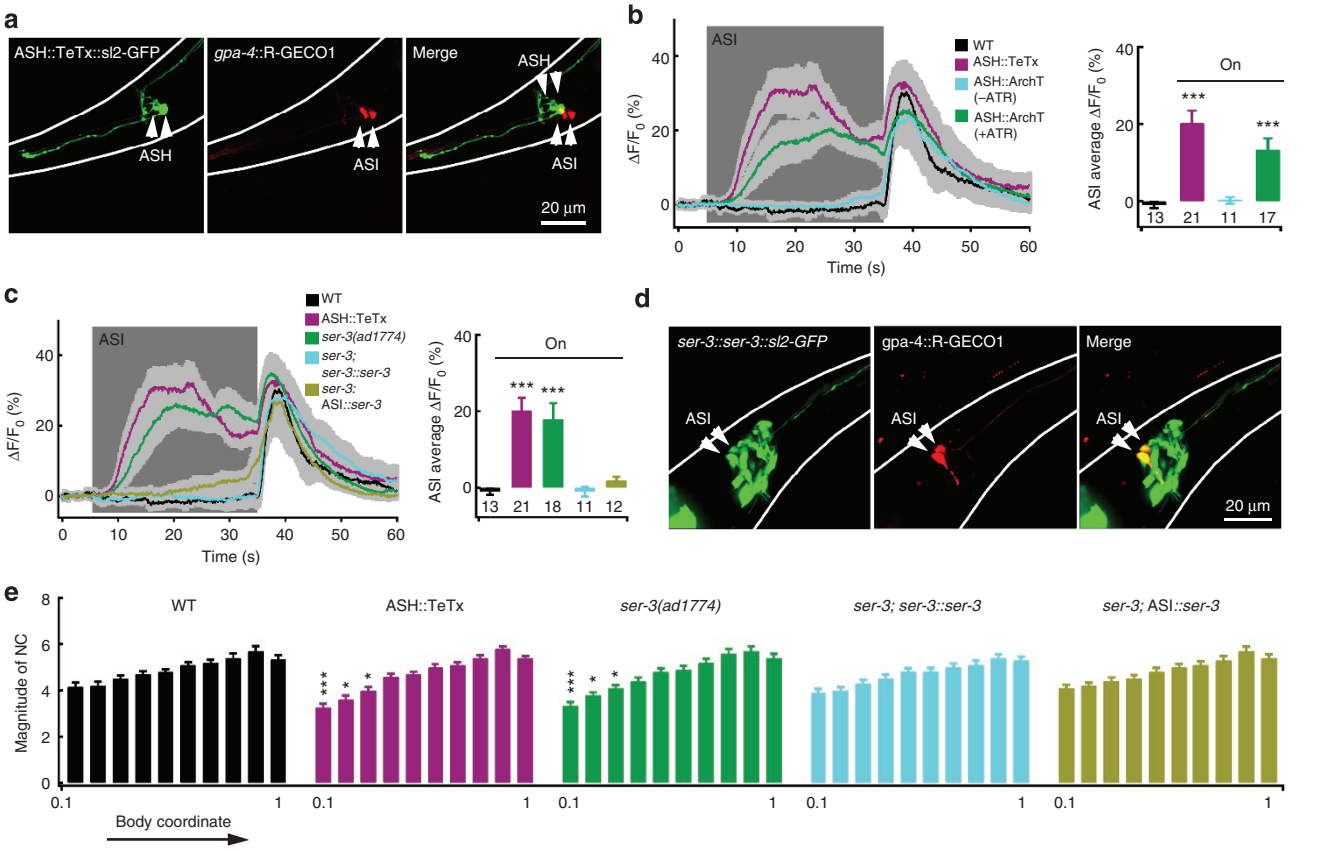

Figure 5 | Octopamine and the SER-3 receptor transduce ASH inhibition to ASIs. (**a**) The specific expression of TeTx in ASH neurons achieved by the use of FLP–FRT site-specific recombination system and R-GECO1 in ASI neurons directed by the *gpa-4* promoter. Scale bars, 20 µm. (**b**) Genetically silencing and optogenetically inhibiting ASHs resulted in a big on-response of Cu^{2+}-evoked Ca^{2+} response in ASI neurons. (**c**) The *ser-3* lof mutation had a similar effect on the ASI response to the 10 mM $CuSO_4$ stimulation as silencing ASHs with TeTx, which could be rescued by extrachromosomal expression of the gene driven by its own or an ASI-specific promoter. (**d**) The expression patterns of *ser-3p::ser-3::sl2-GFP* and *gpa-4p::R-GECO1* in *ser-3*-null animals. These genes were co-expressed in ASI neurons. (**e**) The bending magnitude of the Cu^{2+} avoidance in wild type, mutant and transgenic worms ($n = 30$ assays). All data are expressed as means ± s.e.m. The number on each bar indicates the number of independent tests for each genotype. One-way analysis of variance (ANOVA) test in **b**,**c** and two-way ANOVA test in **e**. Corrected with Bonferroni *t*-test. Values that differ significantly are indicated (*$P \leq 0.05$, **$P \leq 0.01$ and ***$P \leq 0.001$ compared with the wild-type N2 control).

calcium responses to Cu^{2+} were synchronized with those of ASHs (Fig. 6e). More importantly, our analysis of worm Cu^{2+} avoidance behaviour and Cu^{2+} sensitivity (Fig. 6f and Supplementary Fig. 9h–j) confirmed the conclusion derived from the Ca^{2+} data. Altogether, these data support that RICs connect postsynaptically with ASHs and are excited directly by ASHs, and that RICs release OA that directly acts on SER-3 in ASIs to mediate the ASH inhibition of ASIs.

Cross-inhibitory neural circuitry between ASHs and ASIs. We hereby determine that ASI and ASH sensory neurons inhibit reciprocally, and the neurotransmitters 5-HT (released by ADFs) and OA (released by RICs) transduce neuronal signals from these two pairs of sensory neurons by binding their receptors SER-5 and SER-3, respectively. We then used a *ser-5*; *ser-3* double mutation (*ser-3(ad1774) I; ser-5(ok3087) I*) and genetically blocked both ASHs and ASIs, to further confirm the roles of SER-5 and SER-3 signalling pathways in the modulation of Cu^{2+}-elicited Ca^{2+} responses in ASHs and ASIs, as well as worm Cu^{2+}-evoked aversive behaviour. As expected, the double mutation of *ser-3* and *ser-5* affected Cu^{2+}-elicited Ca^{2+} signals of ASH and ASI neurons (Fig. 7a,b and Supplementary Movie 10) similar to the silencing of both ASIs and ASHs (Fig. 7a,b and Supplementary Movie 11). Fortunately, we were able to occasionally record calcium signals in both ASIs and ASHs at the same focal plane of the objective lens (Supplementary Movies 10 and 11), which directly visualized the Ca^{2+} signals of both ASIs and ASHs in the double-blocked worms. We further analysed the avoidance behaviour in the double mutants. Our data showed that the double mutants exhibited similar behavioural defects tested by the dry drop assay to those in the double-silenced worms (Fig. 7c–e and Supplementary Movies 5 and 12). These results suggest that the cross-inhibition between ASHs and ASIs is transduced primarily by 5-HT and OA signalling pathways. We did not examine the Cu^{2+} sensitivity in the double mutants and the double-silenced worms tested by the quadrant assay, as these worms were seriously uncoordinated. Altogether, our study demonstrates that a cross-inhibitory circuit exists between ASH and ASI sensory neurons, which modulates the Cu^{2+} nociception and drives an adaptive avoidance behaviour. The synaptic connections, functional actions and underlying signalling pathways among neurons in the circuit, and the function of the reciprocal inhibition in nociception and aversive behaviour, are summarized in Fig. 7f,g.

Discussion

In the present study, we find that sensory neuron ASIs modulate the ASH Cu^{2+} reception and worm Cu^{2+}-aversive behaviours by cross-inhibition with ASHs, and we dissect the neural circuit

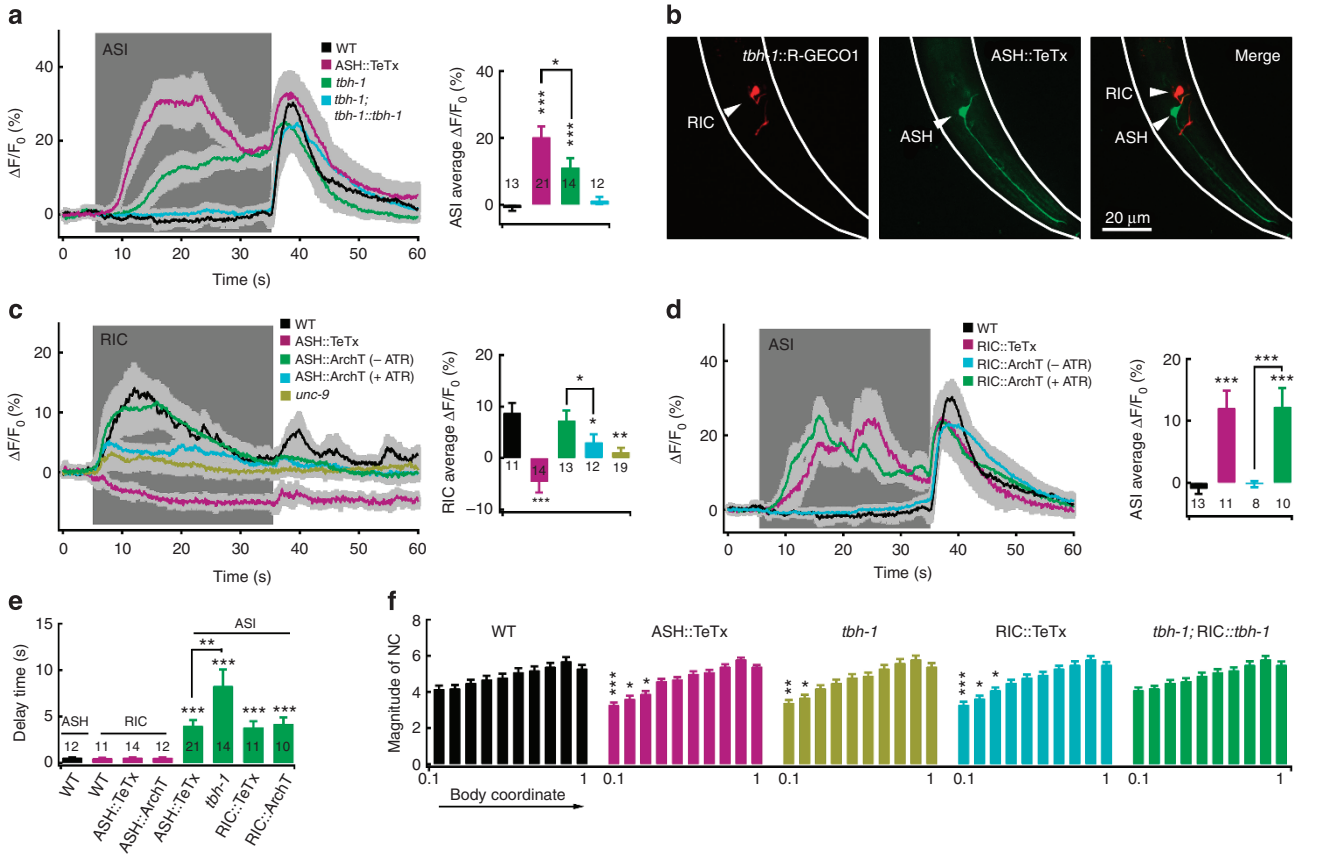

Figure 6 | RIC neurons mediate the inhibition of ASIs by ASHs. (**a**) ASI Ca^{2+} responses to the 10 mM Cu^{2+} stimulation in wild-type, ASH silenced, *tbh-1* mutant and *tbh-1p::tbh-1* rescued worms. (**b**) The expression of R-GECO1 in RIC neurons driven by *tbh-1* promoter and the specific expression of TeTx in ASH neurons realized by the use of the FLP-FRT site-specific recombination system. Scale bar, 20 μm. (**c**) Permanently or temporarily silencing ASH neurons with TeTx or ArchT had a similar effect on RIC Ca^{2+} responses to the 10 mM $CuSO_4$ stimulation. (**d**) ASIs showed an obvious on-response of Cu^{2+}-elicited Ca^{2+} signals after blocking or inhibiting RICs. (**e**) The delay time of Cu^{2+}-evoked calcium transients of ASH, RIC and ASI neurons in worms indicated. The delay time was calculated as the time of stimulus application to the time when the single-exponential fitted curve of individual Ca^{2+} on-response trace cuts fitted straight line of basal Ca^{2+} signals before stimulation. (**f**) The bending magnitude of Cu^{2+}-evoked reversals in wild type, mutant and transgenic worms ($n = 30$ assays). All data are expressed as means ± s.e.m. The number on each bar indicates the number of independent tests for each genotype. One-way analysis of variance (ANOVA) test in **a** and **c**–**e**, and two-way ANOVA test in **f**. Corrected with Bonferroni *t*-test for multiple comparisons. Values that differ significantly are indicated (*$P \leq 0.05$, **$P \leq 0.01$ and ***$P \leq 0.001$ compared with the wild-type N2 control).

and molecular mechanism as shown in Fig. 7f. In this neuronal circuit, ASHs respond to the nociceptive Cu^{2+} stimulus quickly and robustly, which allows ASHs to predominate over and inhibit ASIs at the initial stage. ASI sensory neurons are secondary Cu^{2+} sensory neurons, because they have a weaker Cu^{2+} response. ASI probably release neuropeptides in a state of undetectable Cu^{2+}-induced Ca^{2+} signals in the soma to permit and promote a more rapid onset of Cu^{2+}-evoked activity in ADFs. ADFs are also sensitive to Cu^{2+}, but their activities need permission and promotion from ASIs. Permitted by ASIs and stimulated by Cu^{2+}, ADFs release 5-HT to inhibit ASHs by binding SER-5. The positive and negative manipulation of ASIs, ADFs and both the two pairs of neurons have similar effects on Cu^{2+}-evoked Ca^{2+} signals of ASHs and worm Cu^{2+}-aversive behaviour; besides, the phenotypes of the *tph-1* mutants that have a defect in 5-HT biosynthesis is rescued by ADF-specific expression of the gene (Fig. 4). These data strongly support that ASI → ADF → 5-HT → ASH is a major pathway mediating ASI inhibition of ASHs. However, these data can not completely rule out that ASI could affect ASH by additional pathways. ASI functions as a modulator to suppress hyper-nociception and fine-tune worm avoidance behaviour. This circuit is similar to the central flip-flop circuit that integrates contradictory sensory cues in *C. elegans* feeding regulation[52]. However, there are differences between the two circuits: (1) the central feeding regulatory circuit integrates two different sets of sensory information from the olfactory attractive cues and the gustatory or the olfactory repellents, whereas the peripheral circuit receives the same sensory information from gustatory nociceptive stimuli; (2) the kinetics of the two circuits are different, as the peripheral circuit is biased and progress dependent, whereas the central circuit is bistable and fast switchable, although the nociceptive sensory information has more effects than that of attraction; and (3) their functions are different, in that the central circuit functions to make a rapid decision, whereas the peripheral circuit fine-tunes nociceptive sensation and suppress hyper-responding behaviour.

ASIs inhibit ASHs through the intermediation of ADF sensory neurons that function as interneurons, similar to the functional metamorphosis of AWC^{ON} sensory neuron in the salt sensation circuit[41]. To date, there is no report that shows ADFs are Cu^{2+} sensitive. ADFs are post-synaptic to 8 cells: AWBs (11, the number of synapses) that mediate avoidance to 2-nonanone and 1-octanol, ASHs (5), AWAs (3) that mediate chemotaxis to diacetyl, pyrazine and trimethylthiazole[53], ASEs (1) that mediate avoidance behaviour from Cd^{2+} and Cu^{2+} ion[54], and interneurons AVHs (3), AIYs (1), PVPs (1) and RIH (1).

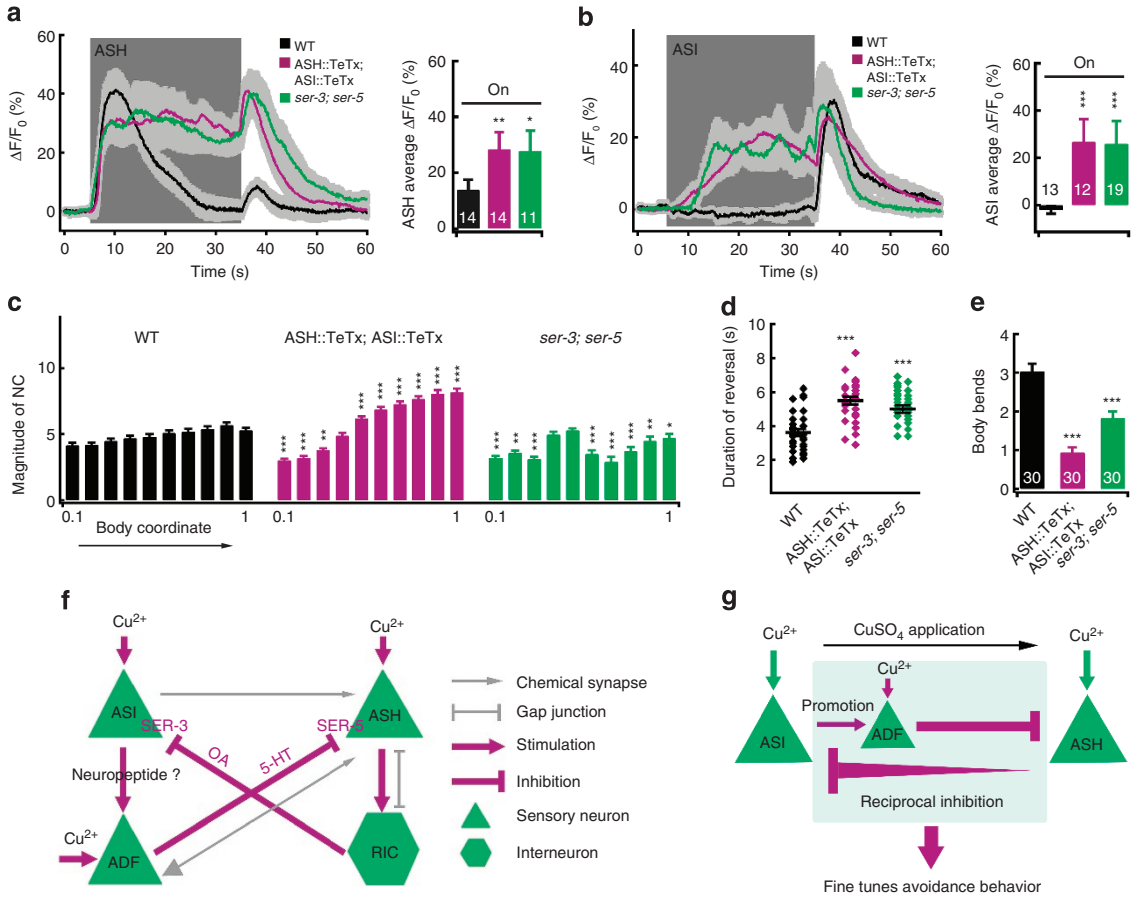

Figure 7 | A dynamic reciprocal inhibition between ASHs and ASIs, and the neuronal circuit. The *ser-3; ser-5* double mutation had a similar effect on ASH (**a**) and ASI (**b**) calcium responses to the 10 mM $CuSO_4$ stimulation as did silencing both the ASH and ASI neurons. (**c**) The bending magnitude along the body centre line in both the ASH and ASI neurons silenced worms and *ser-3; ser-5* double mutants ($n = 30$ assays). The durations (**d**) and body bends (**e**) of the Cu^{2+}-evoked reversals assayed by the dry drop test in worms are indicated. (**f**) Synaptic connections, functional actions and the underlying signalling pathways among neurons in the ASI–ASH reciprocal inhibitory neuron circuit. (**g**) Schematic representation of the cross-inhibition between sensory neuron ASHs and ASIs that fine-tunes nociception and avoidance behaviour. All data are expressed as means ± s.e.m. The number on each bar indicates the number of independent tests for each genotype. One-way analysis of variance (ANOVA) test in **a**,**b** and **d**,**e**, and two-way ANOVA test in **c**. Corrected with Bonferroni *t*-test for multiple comparisons. Values that differ significantly are indicated (*$P \leq 0.05$, **$P \leq 0.01$ and ***$P \leq 0.001$ compared with the wild-type N2 control).

ADF Ca^{2+} signals during $CuSO_4$ stimulation may be a result of neurotransmission from their synaptically connected neuron, particularly from ASHs and ASEs, in addition to the ASIs we identified. However, permanently silencing, opto- and chemo-inhibiting and chemo-activating ASHs had no effect on the ADF Ca^{2+} signals (Supplementary Fig. 5a–h); silencing both ASHs and ASIs postpones the onset of the ADF Ca^{2+} signals similar to blocking ASIs alone (Supplementary Fig. 5i,j); the *unc-13* lof mutation delays the ADF Ca^{2+} onset similar to silencing or inhibiting ASIs (Fig. 4a,b); and with silenced ASIs, $CuSO_4$ evokes Ca^{2+} transients much more efficiently than the chemogenetical activation in ADFs (Supplementary Fig. 4e,f). Collectively, these data show that ADFs receive excitation from ASIs but not from ASHs and are sensitive to Cu^{2+} stimulation, although the detection mechanism needs to be identified. In addition, our data show that ASIs play permission role to promote a more rapid onset of the response in ADF most probably through the intermediation of neurohormonal peptides (Supplementary Fig. 6). Interestingly, why the worm does not employ an ASH→ADF→5-HT→ASH feedback is unclear. We suspect that, first, in a small organism such as *C. elegans* or in a small local area, neuroendocrine is effective as chemical synaptic neurotransmission, especially for the slow kinetic process of sensory modulation. Second, sensational modulation by cross-inhibition using two or multi-information inputs is more adaptive than negative feedback using only one information input. In this work, our data show the ASI neurotransmission in undetectable increases in the soma cytosolic Ca^{2+} levels plays a key role in the reciprocal inhibition. Many sensory neurons do not fire action potentials in response to stimuli. Graded release of neurotransmitters is widely used in sensory neurons, including photoreceptor cells[55], auditory hair cells[56] and olfactory neurons[57]. In *C. elegans*, AWC neurons have non-spiking, have tonic neurotransmitter release at rest and respond to excitatory or inhibitory inputs with graded changes in membrane potential and transmitter release[57]. The possibly tonic neurotransmitter release at rest and graded transmitter release during the stimulation in ASIs need further investigation.

In this study, we use embryonic expression of the clostridial neurotoxin TeTx to permanently block neurotransmission. TeTx is a specific protease of synaptobrevin. The vesicular SNARE protein synaptobrevin is essential for neurotransmitter release and exocytosis of dense-core vesicles[58,59]. Our data show that silencing ASHs with embryonic expression of TeTx has even more significant effects on RIC Ca^{2+} signals than opto-inhibiting ASHs and lof mutation of innexin encoding genes *unc-9* (Fig. 6c)

and *inx-4* (Supplementary Fig. 9f). As there are only gap junctions between ASHs and RICs, these results show embryonic and permanent expression of TeTx not only disrupts the neurotransmitter release via synaptic vesicle fusion with the plasma membrane, but also blocks transmission through gap junctions. One possible explanation is that innexin traffic to the plasma membrane via dense-core vesicles, which is essential for the formation of gap junctions, is interrupted by the permanent expression of the neurotoxin TeTx. Inducible expression of TeTx in adults is needed to resolve this issue.

The gene *tdc-1* encodes the major *C. elegans* tyrosine decarboxylase that is necessary for TA biosynthesis, and *tbh-1* encodes a putative dopamine β-hydroxylase that transforms TA into OA[49,50]. OA and TA have been reported to function independently to modulate many behaviours[14,15,49,50]. In this study, we did not observe more serious defects in the *tdc-1* mutants compared with *tbh-1*-mutated worms. However, our current data are not conclusive enough to exclude the possibility that TA functions in the regulation of the Cu^{2+}-elicited aversive behaviours. Another possible explanation is that TA and OA act antagonistically in response to a Cu^{2+} stimulus as previously suggested[60]. A third hypothesis is that OA biosynthesis in the *tdc-1(n3419) II* mutant may be not fully blocked.

Sensory neurons can be modulated by central and peripheral nervous systems. Peripheral modulations of sensation exist universally in various sensory modalities, including pain, vision and hearing. Disorders of sensory modulation cause diseases. The ASI modulation of ASH-mediated nociception in *C. elegans* determined by this work suppresses the super sensation and super behavioural responses. Our work paves the way to better understand peripheral modulations of the sensations in other animals, including humans.

Methods

Strains. The *C. elegans* strains used in this study are listed in Supplementary Table 1. All strains were maintained and grown according to the standard procedures[49]. The double mutant animals were generated using the standard genetic techniques and confirmed by PCR and sequencing. Most constructs were injected at 30 ng μl^{-1} together with *lin44p::GFP* (5 ng μl^{-1}) as a co-injection marker using the standard techniques. At least five independent lines were examined for each rescue experiment and *in vivo* calcium imaging.

Construction of plasmids and entry clones. Three-Fragment Multisite gateway (Invitrogen, Thermo Fisher Scientific, Waltham, MA, USA) and In-Fusion (Clontech Laboratories, Inc., Mountain View, CA, USA) technology were used to generate the constructs used in this study. Briefly, three entry clones comprising three PCR products (promoter, gene of interest, *sl2-GFP* or *3′UTR*, in name of slot1, slot2 and slot3, respectively) were recombined into the pDEST R4-R3 Vector II or custom-modified destination vectors using *att*L-*att*R (LR) recombination reactions to generate the expression clones.

To construct the slot1 entry clone, the *att*B4-stop-*att*B1r PCR product was recombined with the *att*P4 and *att*P1r sites in the pDONR-P4-P1R vector using the *att*B-*att*P (BP) recombination reactions. A modified vector containing *att*L4-stop-*att*R1 fragment used for the LR recombination reactions was generated. The promoters such as *sra-6p*, *gpa-4p*, *gpa-11p*, *ser-5p*, *tph-1p*, *srh-142p*, *ceh-2p*, *mod-5p*, *ser-3p* and *tbh-1p* were PCR amplified from wild-type N2 genomic DNA and used to substitute for the –stop– fragment in the modified donor vector with the in-fusion method to generate the slot1 entry clones. The length of *sra-6p*, *gpa-4p*, *gpa-11p*, *srh-142p*, *ceh-2p*, *mod-5p*, *ser-5p*, *tph-1p*, *ser-3p*, *tbh-1p* and *unc-9p* are 3.8, 2.5, 3.3, 3.5, 1.6, 4.2, 3.5, 3.7, 2, 4.6 and 2 kb, respectively.

To generate the entry clones slot2 and slot3, we used BP recombination reactions. The *ser-5*, *ser-3* and *tph-1* were PCR amplified from *C. elegans* N2 worm genomic DNA and *tbh-1a* complementary DNA was amplified by PCR with primers containing *att*B1 and *att*B2 reaction sites. The lengths of the PCR products *ser-5*, *ser-3*, *tph-1* and *tbh-1a* are 1,848, 2,230, 2,420 and 1,758 bp, respectively. The BP reaction sites *att*B1 and *att*B2 were inserted into the initiation and terminal sites of the sequences for tetanus toxin light chain (*TeTx*), *R-GECO1*, Archaerhodopsin gene from *Halorubrum* strain TP009 (*ArchT*), *TRVP1*, *HisCl1*, *flp-sl2-flp* and *GFP* using PCR. These PCR fragments flanked by *att*B sites were recombined with the *att*P1 and *att*P2 sites in the pDONR221 vector using BP recombination reactions to generate the entry clone slot2. To generate entry clone slot3, the *sl2-GFP* or *unc-54(3′UTR)* fragments with the inserted BP reaction sites *att*B2r and *att*B3 were recombined with the *att*P2r and *att*P3 sites in the PDONR-P2R-P3 vector using the BP recombination reactions.

Next, we used LR reactions to construct expression plasmids, such as the following: *sra-6p::flp-sl2-flp, sra-6p::R-GECO1, gpa-4p::R-GECO1, gpa-4p::ArchT-GFP, gpa-4p::TeTx::sl2-GFP, gpa-4p::trpv1::sl2-GFP, srh-142p::trpv1::sl2-GFP, ser-5p::ser-5::sl2-GFP, tph-1p::tph-1::sl2-GFP, ceh-2p::R-GECO1, srh-142p::R-GECO1, mod-5p::R-GECO1, srh-142p::TeTx::sl2-GFP, srh-142p::ArchT-GFP, srh-142p::tph-1::sl2-GFP, ser-3p::ser-3::sl2-GFP, gpa-4p::ser-3::sl2-GFP, tbh-1p::tbh-1::sl2-GFP, tbh-1p::R-GECO1, tbh-1p::TeTx::sl2-GFP, tbh-1p::ArchT-GFP* and *unc-9p::GFP*.

To specifically express *TeTx*, *ArchT*, *ser-5*, *TRPV1* and *HisCl1* in ASH neurons, we employed a FLP–FRT site-specific recombination system. We used fusion PCR to get a fragment of *att*B1::*frt-stop-frt-gene::att*B2, then use BP reactions to construct slot2 donor vectors. Using LR reactions, we generated the following listed expression plasmids: *gpa-11p::frt-stop-frt-TeTx::sl2-GFP*, *gpa-11p::frt-stop-frt-ArchT::sl2-GFP*, *gpa-11p::frt-stop-frt-ser-5::sl2-GFP*, *gpa-11p::frt-stop-frt-trpv1::sl2-GFP* and *gpa-11p::frt-stop-frt-HisCl1::sl2-GFP*. Ultimately, the genes of *TeTx*, *ArchT*, *ser-5*, *TRPV1* and *HisCl1* were specifically expressed in ASH neurons through the co-injection of the plasmids *sra-6p::flp-sl2-flp* plus *gpa-11p::frt-stop-frt-TeTx::sl2-GFP*, *sra-6p::flp-sl2-flp* plus *gpa-11p::frt-stop-frt-ArchT::sl2-GFP*, *sra-6p::flp-sl2-flp* plus *gpa-11p::frt-stop-frt-ser-5::sl2-GFP*, *sra-6p::flp-sl2-flp* plus *gpa-11p::frt-stop-frt-TRPV1::sl2-GFP* and *sra-6p::flp-sl2-flp* plus *gpa-11p::frt-stop-frt-HisCl1::sl2-GFP*, respectively.

Confocal fluorescence imaging. All confocal fluorescence imaging was performed using an Andor (Andor Technology plc., Springvale Business Park, Belfast, UK) Revolution XD laser confocal microscope system based on a spinning-disk confocal scanning head CSU-X1 (Yokogawa Electric Corporation, Musashino-shi, Tokyo, Japan), under the control of the Andor IQ 1.91 software. The confocal system was constructed on an Olympus IX-71 inverted microscope (Olympus, Tokyo, Japan). All fluorescent images were imaged by a ×60 objective lens (numerical aperture = 1.45, Olympus) and captured by an Andor iXon^{EM}+ DU-897D EMCCD camera. The images were displayed and analysed using Image J 1.43b software (Wayne Rasband, National Institutes of Health, USA).

Behavioural assays. All the behavioural experiments were performed with young adult animals maintained at 20 °C. The assay plates (3.5 cm nematode growth medium plates (NGM)) were prepared daily. $CuSO_4$ was dissolved in M13 buffer consisting of 30 mM Tris, 100 mM NaCl and 10 mM KCl. To examine a single worm response to Cu^{2+} stimulation, the 'dry drop test' was used[25]. Briefly, a micro-drop (approximately a few hundreds of nanolitres) of Cu^{2+} solution was delivered via a glass micropipette in front of an animal exhibiting forward sinusoidal locomotion, and the rapid backward movement was observed and recorded when the animals encountered the repellent, of which the solution drop had been absorbed into the agar, under a Zeiss Discovery V8 stereomicroscope (Carl Zeiss MicroImaging GmbH, Göttingen, Germany). The image sequences were captured with an Andor iXon^{EM}+ DV885K EMCCD camera. To compare the data from different animals, the quantitative analysis of the behavioural parameters was performed using a custom-written script in MATLAB (Mathworks, Inc., Natick, MA) software. The duration of the reversal was calculated as the time between the initial head reversal and when the tail ceased backward movement. The body bend was defined as the change in the direction of propagation of the part corresponding to the posterior bulb of the pharynx along the *y* axis of the worm, assuming the worm was travelling along the *x* axis. NC was used to quantify the undulatory kinematics of the reversal over time[25,26]. First, the total length of the worm body from head to tail (head = 0; tail = 1) was divided into ten equal segments. Next, the midline of the animal was extracted and divided into 21 equally spaced points from head to tail. The NC of each part of the worm body was subsequently defined by the NC of each even number of points. The mean of absolute value of the NC during a reversal was defined as the magnitude of the NC, corresponding to the bending magnitude. For testing 5-HT and neuron-specific capsaicin activation in the dry drop test, 5-HT (final concentration 5 mM) and capsaicin (final concentration 10 μM) were added to liquid NGM just before pouring to prepare the assay plates. The worms were allowed to rest and adapt to the assay plates for 10–15 min before starting the test.

To examine a mass animal response to $CuSO_4$ stimulus, we used the quadrant assay with some modifications[27]. The worms were washed four times with M13 buffer and placed on the centre of the quadrant assay plates (9 cm NGM plates) (Fig. 1b), which was partitioned into four regions with or without 10 mM $CuSO_4$. For the exogenous capsaicin and 5-HT quadrant assay, the four regions in the tested plate were filled with capsaicin (final concentration 10 μM) and 5-HT (final concentration 5 mM), respectively, which were added into the agar media just before pouring. After 30 min, the numbers of worms over the repellent and control areas were counted. The avoidance index was calculated as (A − B)/(A + B) shown in Fig. 1b, where A is the number of worms over the repellent area and B is the number of worms over the control area.

Calcium imaging. Neuronal calcium responses in the soma were measured by detecting changes in the fluorescence intensity of R-GECO1, a sensitive, rapid kinetic calcium indicator of weak photobleaching[31]. A home-made microfluidic

device was used for calcium imaging as previously described[32,33]. Briefly, a young adult animal was transferred from food to M13 buffer solution to wash food off the body. For exogenous histamine calcium imaging, the worm was transferred from food and starved for 30 min in M13 buffer or M13-histamine solution (final concentration 30 mM)[43]. Then, the worm was loaded into a home-made microfluidic device with its nose exposed to buffer under laminar flow. Stimuli were delivered in M13 buffer with or without $CuSO_4$ (final concentration 10 mM), capsaicin solution (final concentration 100 μM), $CuSO_4$ plus capsaicin and histamine (final concentration 30 mM), using a programmable automatic drug-feeding equipment (MPS-2, InBio Life Science Instrument Co. Ltd, Wuhan, China). R-GECO1 was excited by 525–530 nm light emitted by an Osram Diamond Dragon LTW5AP light-emitting diode (LED) model (Osram, Marcel-Breuer-Strasse 6, Munich, Germany) constructed in a multi-LED light source (MLS102, InBio Life Science Instrument Co. Ltd) and filtered with a Semrock FF01-593/40-25 emission filter (Semrock, Inc., NY, USA), under an Olympus IX-70 inverted microscope (Olympus) equipped with a $\times 40$ objective lens (numerical aperture = 1.3, Zeiss, Germany). Fluorescence images were captured with an Andor iXon$^{EM}+$ DU885K EMCCD camera with a 100-ms exposure time and 256×256 pixels at ten frames per second. The imaging sequences were subsequently analysed using custom-written MATLAB scripts. For Ca^{2+} fluorescence imaging in ASHs, the neurons were exposed under fluorescent excitation light for 1–2 min before recording, to eliminate the light-evoked calcium transients. Each animal was imaged once. The average fluorescence intensity within the initial 5 s before stimulation was taken as basal signal F_0. The per cent changes in fluorescence intensity relative to the initial intensity F_0, $\Delta F = (F–F_0)/F_0 \times 100\%$, were plotted as a function of time for all curves. The mean values of Ca^{2+} signals and s.e.m. were plotted in various colours as indicated and in light grey, respectively, using IGOR Pro 6.10 (Wavemetrics, Portland, OR, USA). 'On' and 'Off' indicate Ca^{2+} signals to the presentation and removal of Cu^{2+} stimulation, respectively. For statistical analysis of the on and off responses, the ΔF and F_0 for the on-response are defined as the fluorescence changes during the application of $CuSO_4$ and the average fluorescence intensity of 5 s before the Cu^{2+} stimulation, and the ΔF and F_0 for off-response are defined as the initial fluorescence changes 5 s after the removal of $CuSO_4$ and the average fluorescence intensity of the last 5 s of the on-response, respectively. The delay time was calculated as the time of stimulus application to the time when the single-exponential fitted curve of individual Ca^{2+} on-response trace cuts fitted straight line of basal Ca^{2+} signals before stimulation.

Optogenetic experiments. To optogenetically inhibit the studied neurons, we used ArchT, a high light-sensitive light-driven outward proton pump, driven by neuron-specific promoters to hyperpolarize the neurons[34]. Worm strains expressing ArchT were raised on 3.5 cm NGM plates seeded with *Escherichia coli* OP50 and All-Trans-Retinal (Sigma, final concentration of 500 μM) or without All-Trans-Retinal as a control. Animals were maintained in the dark unless otherwise indicated. ArchT was excited by 525–530 nm green light emitted by an Osram Diamond Dragon LTW5AP LED model, with adjustable intensity constructed in the MLS102 multi-LED light source.

Statistical data analysis. All statistical analysis was performed using SPSS software V19.0 (IBM, Armonk, NY, USA). We used one-way analysis of variance to test the means among three or more than three samples, and used two-way analysis of variance to determine the significant difference between groups for two factors (that is, the first factor was segment of body, the second factor was strains). Next, we used Bonferroni *t*-test correction for multiple comparisons. The results are presented as the mean values ± s.e.m., with the number of experimental replications (n). Asterisks denote the statistical significance compared with the control: $^{***}P \leq 0.001$; $^{**}P \leq 0.01$; $^{*}P \leq 0.05$.

References

1. Collet, J., Spike, C. A., Lundquist, E. A., Shaw, J. E. & Herman, R. K. Analysis of *osm-6*, a gene that affects sensory cilium structure and sensory neuron function in *Caenorhabditis elegans*. *Genetics* **148,** 187–200 (1998).
2. Olsen, S. R. & Wilson, R. I. Lateral presynaptic inhibition mediates gain control in an olfactory circuit. *Nature* **452,** 956–960 (2008).
3. Root, C. M., Ko, K. I., Jafari, A. & Wang, J. W. Presynaptic facilitation by neuropeptide signaling mediates odor-driven food search. *Cell* **145,** 133–144 (2011).
4. Chalfie, M. *et al.* The neural circuit for touch sensitivity in *Caenorhabditis elegans*. *J. Neurosci.* **5,** 956–964 (1985).
5. Gray, J. M., Hill, J. J. & Bargmann, C. I. A circuit for navigation in *Caenorhabditis elegans*. *Proc. Natl Acad. Sci. USA* **102,** 3184–3191 (2005).
6. Guo, Z. V., Hart, A. C. & Ramanathan, S. Optical interrogation of neural circuits in *Caenorhabditis elegans*. *Nat. Methods* **6,** 891–896 (2009).
7. Piggott, B. J., Liu, J., Feng, Z., Wescott, S. A. & Xu, X. Z. The neural circuits and synaptic mechanisms underlying motor initiation in *C. elegans*. *Cell* **147,** 922–933 (2011).
8. Bargmann, C. I., Thomas, J. H. & Horvitz, H. R. Chemosensory cell function in the behavior and development of *Caenorhabditis elegans*. *Cold Spring Harb. Symp. Quant. Biol.* **55,** 529–538 (1990).
9. Hilliard, M. A. *et al. In vivo* imaging of *C. elegans* ASH neurons: cellular response and adaptation to chemical repellents. *EMBO J.* **24,** 63–72 (2005).
10. Kaplan, J. M. & Horvitz, H. R. A dual mechanosensory and chemosensory neuron in *Caenorhabditis elegans*. *Proc. Natl Acad. Sci. USA* **90,** 2227–2231 (1993).
11. Troemel, E. R., Kimmel, B. E. & Bargmann, C. I. Reprogramming chemotaxis responses: sensory neurons define olfactory preferences in *C. elegans*. *Cell* **91,** 161–169 (1997).
12. Flavell, S. W. *et al.* Serotonin and the neuropeptide PDF initiate and extend opposing behavioral states in *C. elegans*. *Cell* **154,** 1023–1035 (2013).
13. Harris, G. *et al.* The monoaminergic modulation of sensory-mediated aversive responses in *Caenorhabditis elegans* requires glutamatergic/peptidergic cotransmission. *J. Neurosci.* **30,** 7889–7899 (2010).
14. Mills, H. *et al.* Monoamines and neuropeptides interact to inhibit aversive behaviour in *Caenorhabditis elegans*. *EMBO J.* **31,** 667–678 (2012).
15. Wragg, R. T. *et al.* Tyramine and octopamine independently inhibit serotonin-stimulated aversive behaviors in *Caenorhabditis elegans* through two novel amine receptors. *J. Neurosci.* **27,** 13402–13412 (2007).
16. Fielenbach, N. & Antebi, A. *C. elegans* dauer formation and the molecular basis of plasticity. *Genes Dev.* **22,** 2149–2165 (2008).
17. Chen, Z. *et al.* Two insulin-like peptides antagonistically regulate aversive olfactory learning in *C. elegans*. *Neuron* **77,** 572–585 (2013).
18. White, J. Q. & Jorgensen, E. M. Sensation in a single neuron pair represses male behavior in hermaphrodites. *Neuron* **75,** 593–600 (2012).
19. Beverly, M., Anbil, S. & Sengupta, P. Degeneracy and neuromodulation among thermosensory neurons contribute to robust thermosensory behaviors in *Caenorhabditis elegans*. *J. Neurosci.* **31,** 11718–11727 (2011).
20. Bishop, N. A. & Guarente, L. Two neurons mediate diet-restriction-induced longevity in *C. elegans*. *Nature* **447,** 545–549 (2007).
21. Gallagher, T., Kim, J., Oldenbroek, M., Kerr, R. & You, Y. J. ASI regulates satiety quiescence in *C. elegans*. *J. Neurosci.* **33,** 9716–9724 (2013).
22. Hallem, E. A. *et al.* Receptor-type guanylate cyclase is required for carbon dioxide sensation by *Caenorhabditis elegans*. *Proc. Natl Acad. Sci. USA* **108,** 254–259 (2011).
23. Chao, M. Y., Komatsu, H., Fukuto, H. S., Dionne, H. M. & Hart, A. C. Feeding status and serotonin rapidly and reversibly modulate a *Caenorhabditis elegans* chemosensory circuit. *Proc. Natl Acad. Sci. USA* **101,** 15512–15517 (2004).
24. Hilliard, M. A., Bargmann, C. I. & Bazzicalupo, P. *C. elegans* responds to chemical repellents by integrating sensory inputs from the head and the tail. *Curr. Biol.* **12,** 730–734 (2002).
25. Fang-Yen, C. *et al.* Biomechanical analysis of gait adaptation in the nematode *Caenorhabditis elegans*. *Proc. Natl Acad. Sci. USA* **107,** 20323–20328 (2010).
26. Wen, Q. *et al.* Proprioceptive coupling within motor neurons drives *C. elegans* forward locomotion. *Neuron* **76,** 750–761 (2012).
27. Wicks, S. R., de Vries, C. J., van Luenen, H. G. & Plasterk, R. H. CHE-3, a cytosolic dynein heavy chain, is required for sensory cilia structure and function in *Caenorhabditis elegans*. *Dev. Biol.* **221,** 295–307 (2000).
28. Schiavo, G. *et al.* Tetanus and botulinum-B neurotoxins block neurotransmitter release by proteolytic cleavage of synaptobrevin. *Nature* **359,** 832–835 (1992).
29. Macosko, E. Z. *et al.* A hub-and-spoke circuit drives pheromone attraction and social behaviour in *C. elegans*. *Nature* **458,** 1171–1175 (2009).
30. Davis, M. W., Morton, J. J., Carroll, D. & Jorgensen, E. M. Gene activation using FLP recombinase in *C. elegans*. *PLoS Genet.* **4,** e1000028 (2008).
31. Zhao, Y. *et al.* An expanded palette of genetically encoded Ca^{2+} indicators. *Science* **333,** 1888–1891 (2011).
32. Chronis, N., Zimmer, M. & Bargmann, C. I. Microfluidics for *in vivo* imaging of neuronal and behavioral activity in *Caenorhabditis elegans*. *Nat. Methods* **4,** 727–731 (2007).
33. Zhao, X. *et al.* Microfluidic chip-based *C. elegans* microinjection system for investigating cell-cell communication *in vivo*. *Biosens. Bioelectron.* **50,** 28–34 (2013).
34. Han, X. *et al.* A high-light sensitivity optical neural silencer: development and application to optogenetic control of non-human primate cortex. *Front. Syst. Neurosci.* **5,** 18 (2011).
35. Ward, A., Liu, J., Feng, Z. & Xu, X. Z. Light-sensitive neurons and channels mediate phototaxis in *C. elegans*. *Nat. Neurosci.* **11,** 916–922 (2008).
36. Tobin, D. *et al.* Combinatorial expression of TRPV channel proteins defines their sensory functions and subcellular localization in *C. elegans* neurons. *Neuron* **35,** 307–318 (2002).
37. Harris, G. P. *et al.* Three distinct amine receptors operating at different levels within the locomotory circuit are each essential for the serotonergic modulation of chemosensation in *Caenorhabditis elegans*. *J. Neurosci.* **29,** 1446–1456 (2009).
38. Sze, J. Y., Victor, M., Loer, C., Shi, Y. & Ruvkun, G. Food and metabolic signalling defects in a *Caenorhabditis elegans* serotonin-synthesis mutant. *Nature* **403,** 560–564 (2000).
39. Richmond, J. E., Davis, W. S. & Jorgensen, E. M. UNC-13 is required for synaptic vesicle fusion in *C. elegans*. *Nat. Neurosci.* **2,** 959–964 (1999).

40. Tokumaru, H. & Augustine, G. J. UNC-13 and neurotransmitter release. *Nat. Neurosci.* **2,** 929–930 (1999).
41. Leinwand, S. G. & Chalasani, S. H. Neuropeptide signaling remodels chemosensory circuit composition in *Caenorhabditis elegans*. *Nat. Neurosci.* **16,** 1461–1467 (2013).
42. Thiele, T. R., Faumont, S. & Lockery, S. R. The neural network for chemotaxis to tastants in *Caenorhabditis elegans* is specialized for temporal differentiation. *J. Neurosci.* **29,** 11904–11911 (2009).
43. Pokala, N., Liu, Q., Gordus, A. & Bargmann, C. I. Inducible and titratable silencing of *Caenorhabditis elegans* neurons *in vivo* with histamine-gated chloride channels. *Proc. Natl Acad. Sci. USA* **111,** 2770–2775 (2014).
44. Avery, L., Bargmann, C. I. & Horvitz, H. R. The *Caenorhabditis elegans unc-31* gene affects multiple nervous system-controlled functions. *Genetics* **134,** 455–464 (1993).
45. Lin, X. G. *et al.* UNC-31/CAPS docks and primes dense core vesicles in *C. elegans* neurons. *Biochem. Biophys. Res. Commun.* **397,** 526–531 (2010).
46. Kass, J., Jacob, T. C., Kim, P. & Kaplan, J. M. The EGL-3 proprotein convertase regulates mechanosensory responses of *Caenorhabditis elegans*. *J. Neurosci.* **21,** 9265–9272 (2001).
47. Jacob, T. C. & Kaplan, J. M. The EGL-21 carboxypeptidase E facilitates acetylcholine release at *Caenorhabditis elegans* neuromuscular junctions. *J. Neurosci.* **23,** 2122–2130 (2003).
48. White, J. G., Southgate, E., Thomson, J. N. & Brenner, S. The structure of the nervous system of the nematode *Caenorhabditis elegans*. *Philos. Trans. R. Soc. Lond. B. Biol. Sci.* **314,** 1–340 (1986).
49. Alkema, M. J., Hunter-Ensor, M., Ringstad, N. & Horvitz, H. R. Tyramine Functions independently of octopamine in the *Caenorhabditis elegans* nervous system. *Neuron* **46,** 247–260 (2005).
50. Chase, D. L. & Koelle, M. R. Biogenic amine neurotransmitters in *C. elegans*. WormBook. ed. The *C. elegans* Research Community, WormBook, http://www.wormbook.org (2007).
51. Altun, Z. F., Chen, B., Wang, Z. W. & Hall, D. H. High resolution map of *Caenorhabditis elegans* gap junction proteins. *Dev. Dyn.* **238,** 1936–1950 (2009).
52. Li, Z. *et al.* Dissecting a central flip-flop circuit that integrates contradictory sensory cues in *C. elegans* feeding regulation. *Nat. Commun.* **3,** 776 (2012).
53. Bargmann, C. I., Hartwieg, E. & Horvitz, H. R. Odorant-selective genes and neurons mediate olfaction in *C. elegans*. *Cell* **74,** 515–527 (1993).
54. Sambongi, Y. *et al.* Sensing of cadmium and copper ions by externally exposed ADL, ASE, and ASH neurons elicits avoidance response in *Caenorhabditis elegans*. *Neuroreport* **10,** 753–757 (1999).
55. Heidelberger, R. Mechanisms of tonic, graded release: lessons from the vertebrate photoreceptor. *J. Physiol.* **585,** 663–667 (2007).
56. Johnson, S. L. *et al.* Synaptotagmin IV determines the linear Ca^{2+} dependence of vesicle fusion at auditory ribbon synapses. *Nat. Neurosci.* **13,** 45–52 (2010).
57. Chalasani, S. H. *et al.* Dissecting a circuit for olfactory behaviour in *Caenorhabditis elegans*. *Nature* **450,** 63–70 (2007).
58. Banfield, D. K., Lewis, M. J. & Pelham, H. R. A SNARE-like protein required for traffic through the Golgi complex. *Nature* **375,** 806–809 (1995).
59. Ilardi, J. M., Mochida, S. & Sheng, Z. H. Snapin: a SNARE-associated protein implicated in synaptic transmission. *Nat. Neurosci.* **2,** 119–124 (1999).
60. Roeder, T., Seifert, M., Kahler, C. & Gewecke, M. Tyramine and octopamine: antagonistic modulators of behavior and metabolism. *Arch. Insect Biochem. Physiol.* **54,** 1–13 (2003).

Acknowledgements

We thank *Caenorhabditis* Genetic Center (CGC) and National BioResource Project (NBRP) for strains, and Dr B.F. Liu for support of fabrication of microfluidic devices, Dr C. Bargmann for CX8060 and CX9317 strains and cDNA of HisCl1, Dr E.M. Jorgensen for TeTx, Dr J. Yao for rat TRPV1 cNDA, Dr K. Deisseroth for ArchT, and Dr R.E. Campbell for R-GECO1.0. This work was supported by grants from the Major State Basic Research Program of P.R. China (2011CB910200 and 2010CB833700), the National Science Foundation of China (J1103514) and the Fundamental Research Funds for the Central Universities (2014TS083).

Author contributions

M.G. and T.H.W. performed the majority of the behaviour and imaging experiments. Y.-X.S, M.-H.G., C.M.S., W.P.N, L.L.L. and M.T.H.A.M. constructed the plasmids. Z.J.X., C.L.G. and S.P.W. carried out some of behaviour experiments. Z.X.W. and M.G. conceived the experiments, interpreted the data and wrote the manuscript with help from all of the other authors. Z.X.W. supervised the project.

Additional information

Supplementary Information accompanies this paper at http://www.nature.com/naturecommunications

Competing financial interests: The authors declare no competing financial interests.

Reprints and permission information is available online at http://npg.nature.com/reprintsandpermissions/

How to cite this article: Guo, M. *et al.* Reciprocal inhibition between sensory ASH and ASI neurons modulates nociception and avoidance in *Caenorhabditis elegans*. *Nat. Commun.* 6:5655 doi: 10.1038/ncomms6655 (2015).